Chemical Equilibrium and Isotope Temperatures[1]

J. Pochodzalla
Max-Planck-Institut für Kernphysik, D-69117 Heidelberg, Germany
and
W. Trautmann
Gesellschaft für Schwerionenforschung mbH, D-64291 Darmstadt, Germany

ABSTRACT

The measurement and interpretation of isotopic yield ratios in heavy ion reactions at intermediate and high energies are discussed and the usefulness of these observables for establishing equilibrium properties and for determining thermodynamic parameters is illustrated. The examples are mainly taken from work performed with lighter projectiles at intermediate and high energies and from studies of spectator reactions at relativistic energies. As an application, the caloric curve of nuclei, as derived for Au on Au collisions, is introduced and discussed.

[1] to appear in "Isospin Physics in Heavy-Ion Collisions at Intermediate Energies" Eds. Bao-An Li and W. U. Schröder, Nova Science Publishers, Inc., in preparation

15.1 Introduction

Isotopic yield ratios have proven to be useful observables for studying the mechanisms of heavy-ion reactions at intermediate and high energies. Production yields for isotopically resolved particles and nuclear fragments and combinations thereof can provide us with answers to the questions of mutual stopping and subsequent equilibration of the collision partners. To the extent that equilibrium is reached, they permit the extraction of the corresponding thermodynamical variables. The entropy, density, and particularly the temperature of the ensemble of excited nuclear systems, formed in the course of energetic encounters, have been deduced from measured isotopic yield ratios. These parameters provide a characterization of heavy-ion reactions whose complex dynamics advocate a global description in statistical terms. Temperature observables and their correlation with the excitation energy, commonly termed caloric curve of nuclei, offer the possibility to explore the link between the liquid-gas phase transition predicted for infinite nuclear matter and the decay properties of finite nuclei.

The examples considered in this chapter are heavy-ion reactions at bombarding energies in the range of about 100 MeV per nucleon up to a few GeV per nucleon. The dynamics of these reactions, high above the Fermi energy, are predominantly governed by nucleon-nucleon collisions and by the possibility of the production (and reabsorption) of secondary particles, mostly pions. Nuclear matter properties are being probed at densities far away from the ground state density and at excitation energies up to the binding limit of nuclear matter and beyond. The corresponding part of the phase diagram of extended nuclear matter includes the spinodal and coexistence regions of the phase transition from the normal liquid phase to a gas-like phase consisting of nucleons and light complex particles. Consequences of these nuclear phase properties are expected and searched for in this class of reactions.

The isotopic degrees of freedom in the nuclear disassembly and their role in a statistical description will be the primary subject of this chapter. Isospin, therefore, will not appear here in its role as a symmetry principle of nuclear structure that follows from the charge independence of the nuclear forces. The third component of the isospin, $t_3 = (N - Z)/2$, is simply used to characterize isotopes according to their neutron and proton numbers N and Z. Isospin equilibration, consequently, will indicate that isotopic yield distributions correspond to the expectations for chemical equilibrium. Isospin equilibration, in this sense, is a consequence of chemical equilibration and as such a necessary condition for equilibrium that can be tested experimentally.

The experimental determination of the mass number A of a reaction product is, generally, more difficult than the determination of the element number Z alone. It involves either improved resolutions, if the $\Delta E - E$ technique is used, or measurements of additional quantities, such as the time-of-flight or the magnetic rigidity of the emitted reaction product. Yield ratios of neighboring isotopes, in return, may be assumed to be little influenced by dynamical effects such as Coulomb, recoil, or size effects, and thus should permit a fairly unbiased look at the balance equation

$$(A+1, Z) \longleftrightarrow (A, Z) + n. \tag{15.1}$$

In a statistical description this balance is determined by the temperature and the chemical potentials, the measurement thus gives access to these equilibrium parameters.

We will begin this chapter with a discussion of some of the earlier experiments on isotopic effects, performed with beams of fairly light ions of intermediate energy and of light particles at high energies in the GeV range. These data will allow us to make the distinction between isospin mixing and isospin equilibration. We will then more generally discuss equilibrium in spectator reactions with heavier ions of incident energies up to one GeV per nucleon. The determination of equilibrium parameters, in particular of the temperature, and the construction of a caloric curve of nuclei will be described in the final sections of this chapter.

15.2 Isospin Mixing and Equilibration

One of the earlier experiments on isotopic degrees of freedom has been conducted at the CERN synchrocyclotron during the eighties of the last century [1]. In this experiment, the isotopic composition of decay products was studied as a function of the neutron-to-proton (N/Z) content of nuclear systems over the range accessible with stable projectile and target nuclei. Targets of ^{58,64}Ni, $^{\mathrm{nat}}$Ag, and ^{197}Au were bombarded with ^{12}C and ^{18}O beams with incident energy 84 MeV per nucleon. The produced particles and fragments were measured inclusively with high-resolution telescopes placed at several angles between $\theta_{\mathrm{lab}} = 40°$ and $120°$. Each telescope consisted of an axial-field

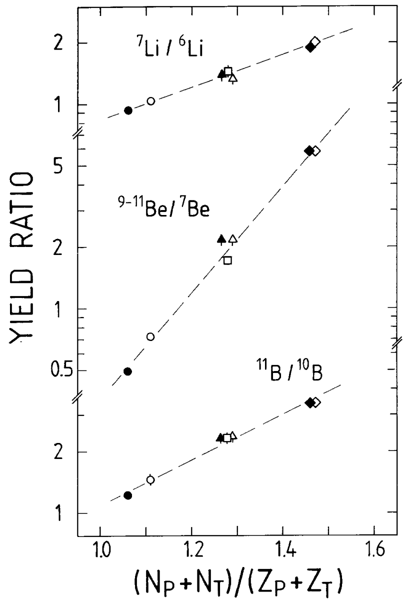

Figure 15.1: Ratios of energy-integrated isotope yields, measured at $\theta_{\rm lab} = 40°$, as functions of the N/Z ratio of the combined system of projectile and target. Closed and open symbols denote ^{12}C and ^{18}O projectiles, respectively; circles, squares, triangles, and diamonds stand for ^{58,64}Ni, $^{\rm nat}$Ag, and ^{197}Au targets (from Ref. [1]).

ionization chamber followed by three silicon detectors of increasing thickness and a bismuth germanate scintillation detector. Full isotope separation for ions up to carbon was achieved for fragment energies $E/A \geq 3$ MeV and for ions up to beryllium at somewhat lower energies.

Energy-integrated isotope yields were obtained by extrapolating from the isotopically resolved parts of the energy spectra with the help of fitting functions which were derived from the model of a Maxwellian source moving in beam direction. The measured isotope ratios were found to vary little with the detection angle. The following discussion is therefore based on the data measured at $\theta_{\rm lab} = 40°$ which have the highest statistics and the smallest experimental uncertainties. This angle is also sufficiently backward to be outside the range of projectile fragmentation.

Three yield ratios, of lithium, beryllium, and boron isotopes and for all the investigated reactions, are shown in Fig. 15.1, plotted as functions of the neutron-to-proton ratio N/Z of the combined system of projectile and target nuclei. This way of representing the data was motivated by the following observations: The isotope-yield ratios vary strongly with the choice of the target. The relevant property of the target, however, is neither the mass number A nor the atomic number Z but rather the ratio N/Z; the yield ratios are different for the ^{58}Ni and ^{64}Ni targets but, apparently, the same for the ^{64}Ni and $^{\rm nat}$Ag targets which have equal N/Z. Furthermore, the different N/Z of the ^{12}C and ^{18}O projectiles seem to have little influence except in the reactions with the ^{58}Ni target. The fact that in this case the ratio measured with the ^{12}C projectiles are significantly smaller than those measured with ^{18}O suggests that the N/Z of the combined system rather than that of the target nucleus alone is the relevant ordering parameter. Plotted in this way, all three isotope-yield ratios follow smooth exponential functions and increase monotonically with N/Z (Fig. 15.1).

We may first conclude that the combined system of the projectile and the whole target is involved in the process of emission of complex fragments in these reactions. For the moment, we will call this complete mixing, as expected for projectile nuclei that are completely stopped in the target prior to the fragment emission. The two collision partners are thought to form a sufficiently homogeneous system such that the individual contributions of the projectile and target can no longer be separately identified. Even though confirmed for a variety of reactions [2, 3] this is by no means a trivial result; there are many examples for which complete mixing is not observed: Isotope yield ratios of projectile fragments measured at small angles with ^{12}C beams at the same energy 84 MeV per nucleon are virtually constant for the same range of targets [4]. Similar observations were made at GANIL where the fragmentation of heavier projectiles was studied [5, 6, 7]. For the set of reactions with $A = 40$ projectiles and $A = 58$ targets, discussed in detail by Li and Yennello in Chapter 19, the stopping is found to become incomplete at incident energies of 45 MeV per nucleon and above [8, 9, 10]. For the mass symmetric reactions with ^{96}Zr and ^{96}Ru projectiles and targets, studied at the much higher energy of 400 MeV per nucleon, the mixing was found to increase with the centrality of the collision but to remain incomplete even at the smallest impact parameters (Ref. [11] and Chapter 19).

Incomplete mixing has even been observed in the same set of reactions at 84 MeV per nucleon with ^{12}C and ^{18}O projectiles, as illustrated in Fig. 15.2. There the ratios of hydrogen isotopes from the preequilibrium component measured at $\theta_{\rm lab} = 40°$ are shown for different mixing assumptions. With

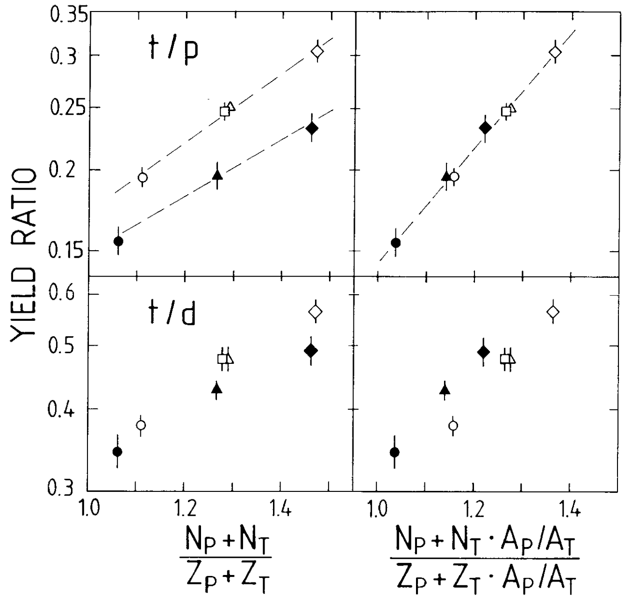

Figure 15.2: Ratios of preequilibrium triton-to-proton yields (top) and triton-to-deuteron yields (bottom), measured at $\theta_{\text{lab}} = 40°$ and plotted as functions of the N/Z ratio of the combined system (left-hand side) and of a source consisting of equal numbers of nucleons from the projectile and from the target (right-hand side). The symbols are chosen as in Fig. 15.1 (from Ref. [1]).

the postulate that the observed ratios should be a unique function of the N/Z ratio of the emitting source, the light particle data are inconsistent with emission from the combined system (Fig. 15.2, left panels). The t/p ratios can be reconciled with this postulate if the emitting source is assumed to consist of equal numbers of nucleons from the projectile and from the target, chosen according to their respective N/Z ratios (Fig. 15.2, upper right panel). For the t/d ratios the same assumption overcorrects the deviations (lower right panel) but by mixing projectile and target nucleons with the ratio 1:2 a unique and monotonic increase of the measured isotope ratios can be achieved. These examples show that preequilibrium light particles originate from subsystems considerably smaller than the combined system of projectile and target.

The question of isospin equilibration will now be addressed by asking for the significance of the slopes characterizing the dependence of the isotope ratios on the source N/Z. Their trends can be most easily understood by considering the grand canonical approach [12, 13, 14]. Here the yield ratios of neighboring isotopes can be expressed as

$$\frac{Y(A+1,Z)}{Y(A,Z)} = (\frac{A+1}{A})^{3/2} \cdot \frac{\omega(A+1,Z)}{\omega(A,Z)} \cdot \exp(\frac{\mu_{\rm n} + \Delta B}{T}) \qquad (15.2)$$

where $\omega(A,Z)$ denotes the internal partition function and ΔB is the difference of the binding energies of the two nuclides. The chemical potentials $\mu_{\rm n}$ of neutrons and $\mu_{\rm p}$ of protons guarantee the conservation of the mean mass and charge of the disassembling nucleus within a given volume and, therefore, are functions of the N/Z ratio of the system. The assumption that $\mu_{\rm n}$ depends, to first order, linearly on N/Z immediately explains the experimental finding that the logarithm of the ratio increases linearly with the N/Z ratio of the emitting source. It further explains why the slopes are about the same for the pairs of lithium and boron isotopes which both differ by one neutron (Fig. 15.1). The ^{7}Be isotope is, at least, two neutrons lighter than the most abundant heavier isotope, and a term $2 \cdot \mu_{\rm n}/T$ (or higher) appears in the exponent on the right-hand side of Eq. 15.2. Consequently, the slopes should be about twice as large which is also in agreement with the observation. For this qualitative consideration, it has been tacitly assumed that the temperature T is approximately the same for the considered fragment species and reactions, a condition that is furthermore needed for ensuring constancy of the ratios of the internal partition functions. It will be shown below that this assumption is not unrealistic in the present case (Section 15.6).

It is an instructive exercise to estimate the N/Z dependence expected from other conceivable mechanisms [15]. In particular, the binomial distribution following from the assumption of a combinatorial mechanism of fragment formation yields a variation in proportion to $N/(N+Z)$ for ratios of neighboring isotopes which is by far too weak to describe the data. The observed dramatic variation of the isotope ratios with N/Z is a consequence of the exponential dependence on the ratio $\mu_{\rm n}/T$ and thus may by itself indicate chemical equilibrium. Equilibrium in this sense does not necessarily imply complete mixing. The equilibration may be local as in the examples of incomplete mixing discussed above where strong variations as a function of the neutron-to-proton ratio of the assumed localized sources were observed. Global equilibrium, clearly, requires complete mixing.

15.3 The Isotopic Effect

An alternative possibility to study isospin equilibration is provided by the so-called isotopic effect [16, 17]. It is generally defined as the net effect observed when switching to another target made from a different isotope of the same element with no other change of the experimental conditions. Here we will specifically consider ratios of production cross sections of particular fragment species in otherwise identical reactions on the tin isotopes with $A = 112$ and $A = 124$. These isotopes have been frequently chosen as targets and, more recently, also as beams for isotopic studies ([18, 19, 20] and references given in [17]).

For the case of ^{112}Sn and ^{124}Sn targets and, e.g., the production of ^{7}Li fragments we may write

$$\delta(^{7}\mathrm{Li}) = \frac{\sigma(^{7}\mathrm{Li};^{112}Sn)}{\sigma(^{7}\mathrm{Li};^{124}Sn)} = \frac{\sigma(^{7}\mathrm{Li};N/Z = 1.24)}{\sigma(^{7}\mathrm{Li};N/Z = 1.48)} = \delta(^{7}\mathrm{Li};\Delta(N/Z) = 0.24). \tag{15.3}$$

This notation emphasizes the role of the N/Z ratio of the source as the dominant parameter. It ignores the contribution of the projectile to the source which, however, may be justified for the very light projectiles (p, d, α) that were used in the examples to be discussed in the following. By defining a reduced isotopic effect $\delta(X)/\delta(^{6}\mathrm{Li})$, i.e. the isotopic effect for species X in relation to that for ^{6}Li, uncertainties of the absolute normalizations of the measurements with the two targets are eliminated. The reduced isotopic effect represents a double ratio which, e.g., for X = ^{7}Li is equal to the ratio of the ^{7}Li/^{6}Li yield ratios measured with the two targets. It is an observable equivalent to the value of the slope of the ^{7}Li/^{6}Li yield ratio as a function of N/Z (Fig. 15.1).

Figure 3 shows the reduced isotopic effects measured at the proton synchrotron of the JINR, Dubna, for the interaction of protons of $E_{\mathrm{p}} = 6.7$ GeV with the target nuclei ^{112}Sn and ^{124}Sn [21]. These experiments were performed inclusively with multi-element telescopes positioned at approximately 90° with respect to the beam. The cross section ratios differ by more than one order of magnitude for the neutron poor and the most neutron rich fragments. Plotted against the third component t_3 of the fragment isospin, the data exhibit a nearly perfect exponential dependence. This result is a generalization of what was observed for the slopes of isotope ratios (Fig.

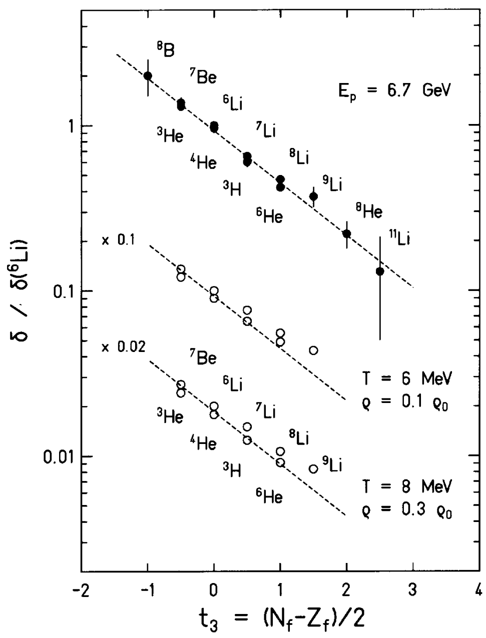

Figure 15.3: Reduced isotopic effect $\delta/\delta(^6\text{Li})$ versus the third component of the isospin t_3. The experimental results for protons of $E_p = 6.7$ GeV [21] are given in the upper part (full circles). The dashed line represents an exponential fit to the data. In the lower part the same fit curve is compared to the results obtained with the quantum-statistical model (open circles), calculated with two sets of parameters T and ρ, and with $\Delta(N/Z) = 0.24$ (ρ_0 denotes the saturation density of nuclei, from Ref. [17]).

15.1) and can also be understood on the basis of Eq. 15.2.

Quantum-statistical models (QSM) are useful for extracting more quantitatively the information contained in measured isotope yield ratios or isotopic effects. Several versions of such models have been developed for different purposes [22, 23, 24, 25]. For the following comparison the model of Hahn and Stöcker [22] has been chosen. It assumes thermal and chemical equilibrium at the breakup point where the fragmenting system is characterized by a density ρ, temperature T, and by its overall N/Z ratio. The model respects fermion and boson statistics which, however, is not crucial at high temperature. It does not make provisions for the finite size of nuclear systems but follows the sequential decay of excited fragments according to tabulated branching

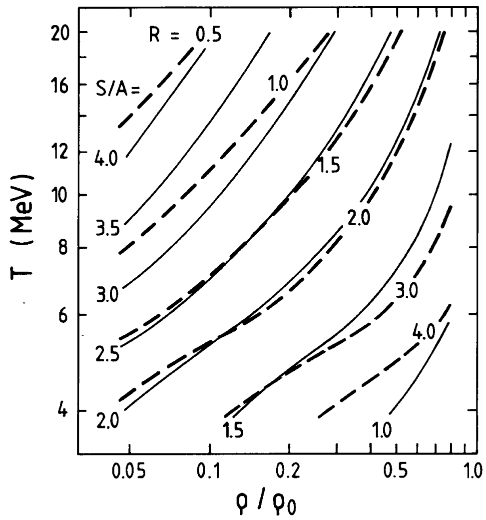

Figure 15.4: Results of calculations with the quantum-statistical model code [22] for the composite system ^{12}C + ^{197}Au. The thin full lines are the isentropes in the temperature-versus-density plane. The thick dashed lines are the contours of constant ratio R of the yields for ^{7}Li and ^{6}Li (from Ref. [15]).

ratios.

Results of QSM calculations are given in the lower half of Fig. 15.3. They are compared to the experimental data represented by the dashed exponential fit curves. Pairs of temperatures T and densities ρ can apparently be found that give an accurate description of the observed t_3 dependence. The temperatures chosen in these examples are in the range of measured breakup temperatures (see below), and the matching densities correspond to large breakup volumes as assumed in the statistical multifragmentation models [26, 27]. Low densities in this range have been deduced from proton-proton correlation functions measured for reactions in which multifragmentation is dominant [28]. Their meaning in the light-ion induced reactions with small mean fragment multiplicities [29] is not fully clear at present.

The example illustrates that isotopic effects or isotopic yield ratios in this way do not permit the individual determination of either the breakup temperature or density but rather define a relation between them. This was studied in more detail in Refs. [1, 15, 30] where it was found that the loci in the temperature-versus-density plane corresponding to fixed isotopic yield ratios effectively coincide with isentropes (Fig. 15.4). Obviously, the N/Z ratio of the system has to be specified if this is to be used as a method to determine the entropy at breakup. Entropy values S/A determined in this way for fragmentation channels in ^{12}C and ^{18}O induced reactions at bombarding energies up to 84 MeV per nucleon are in the range of 1.5 to 2.5 [1, 30]. More recent analyses based on similar methods have shown that this range of entropies is virtually an invariant over a wide variety of fragmentation reactions [17, 31]. The interest attracted by the entropy as an observable in heavy ion reactions is related to the approximately isentropic nature of the expansion phase [32, 33]. Entropy measurements thus permit a characterization of the excited systems formed during the initial impact and before expansion [22].

15.4 Equilibrium in Spectator Reactions

In this section we will temporarily lift the restriction to isotopic degrees of freedom and more generally search for observables with the potential of giving further evidence for equilibrium in fragmentation reactions. We will also proceed to a new type of reaction and investigate spectator decays initiated by collisions of heavy nuclei at relativistic bombarding energies [34]. These reactions are best viewed within the participant-spectator model [35] which distinguishes between the 'hot' hadronic system, formed by fast nucleons and secondary hadrons produced in hard collisions, and the 'cold' spectators consisting of the remnants of the incident nuclei. It turns out that these spectators can also be quite highly excited, up to and beyond their total binding energies. Because of the nature of the excitation mechanism, predominantly nucleon knockout and absorption of slow nucleons recoiling from hard collisions, high degrees of equilibration may be expected.

We will focus on two recent experiments with the ALADIN spectrometer at the heavy-ion synchrotron SIS of the GSI Darmstadt in which reactions of ^{197}Au + ^{197}Au in the regime of relativistic energies up to 1 GeV per nucleon were studied. In the first experiment, the ALADIN spectrometer was used to detect and identify the products of the projectile-spectator decay [36]. The setup offers full coverage for projectile fragments with a dynamic range extending from helium isotopes to the original projectiles. Individual charge resolution and, for lighter fragments up to $A \approx 20$, also individual mass resolution is obtained. The Large-Area Neutron Detector (LAND) was

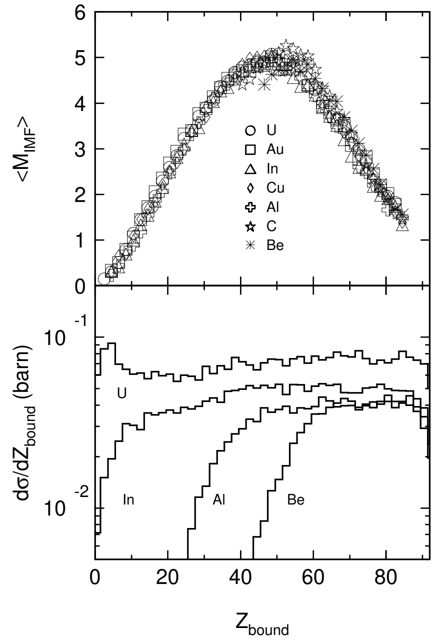

Figure 15.5: Top: Mean multiplicity of intermediate-mass fragments $\langle M_{\mathrm{IMF}} \rangle$ as a function of Z_{bound} for the reactions of ^{238}U projectiles at $E/A = 1000$ MeV with the seven targets Be, C, Al, Cu, In, Au, and U. Bottom: Measured cross sections $d\sigma/dZ_{\mathrm{bound}}$ for the reactions of ^{238}U projectiles at $E/A = 1000$ MeV with the four targets Be, Al, In, and U. Note that the experimental trigger suppresses the very peripheral collisions at $Z_{\mathrm{bound}} \geq 70$ which have much larger cross sections than indicated here (from Ref. [36]).

used to measure coincident free neutrons emitted by the projectile source. In the second experiment, three multi-detector hodoscopes, consisting of a total of 216 Si-CsI(Tl) telescopes, and three high-resolution telescopes were positioned at backward angles to measure the yields and correlations of isotopically resolved light fragments of the target-spectator decay [37]. From these data excitation energies and masses, temperatures, and densities were deduced.

For the presentation of these data, the quantity Z_{bound} has emerged as a useful sorting variable. Z_{bound} is equal to the sum of the atomic numbers Z_i of all projectile fragments with $Z_i \geq 2$. It reflects the variation of the charge of the primary spectator system and is therefore correlated with the impact

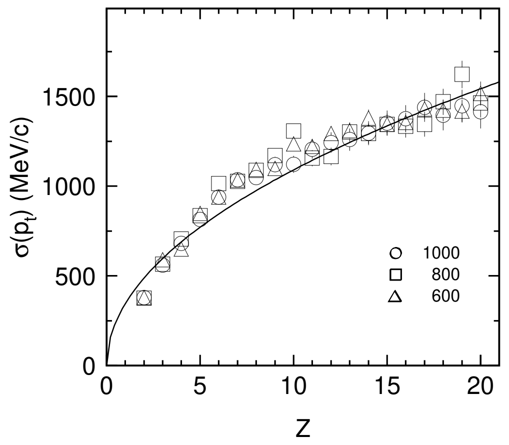

Figure 15.6: Widths of the transverse-momentum distributions $\sigma(p_t)$ as a function of the fragment atomic number Z for the reactions ^{197}Au + ^{197}Au at $E/A = 600$, 800, and 1000 MeV and for $20 \leq Z_{\text{bound}} \leq 60$. The line is proportional to $\sqrt{Z}$ (from Ref. [36]).

parameter of the reaction. In the second type of experiments, with high-resolution detectors looking at the target spectator, the symmetric collision system ^{197}Au + ^{197}Au was studied. Z_{bound} was determined for the projectile decay with the time-of-flight wall of the ALADIN spectrometer, and it was assumed that its mean values for the target and projectile spectators are identical for a given event class.

The universal features of the spectator decay, as apparent in the observed Z_{bound} scaling of the measured charge correlations, were the first and perhaps most striking indications for equilibrium [36]. The target invariance of the M_{IMF} versus Z_{bound} correlation was first observed for collisions of ^{197}Au projectiles with C, Al, Cu, and Pb targets at 600 MeV per nucleon [38, 39]. In Fig. 15.5 (top) this correlation is shown for ^{238}U projectiles at 1000 MeV per nucleon and for a set of seven targets, ranging from Be to U. The data for the lighter targets extend only over parts of the Z_{bound} range, more clearly visible in the bottom part of the figure where the differential cross sections $d\sigma/dZ_{\text{bound}}$ for four out of the seven targets are displayed. From the cross sections, by assuming a monotonic relation between Z_{bound} and the impact parameter, an empirical impact parameter scale can be obtained. Central collisions lead to the smallest values of Z_{bound} that can be reached with a

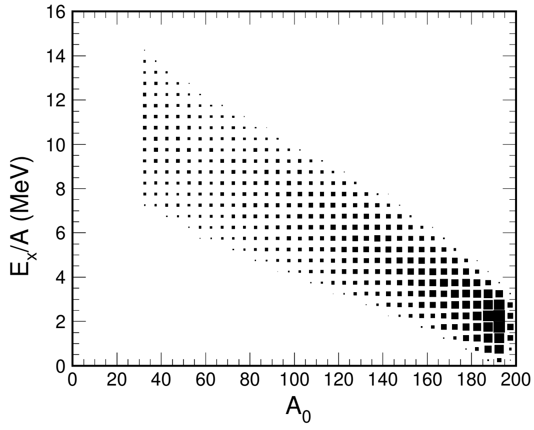

Figure 15.7: Ensemble of excited spectator nuclei used as input for the calculations with the statistical multifragmentation model as a function of their excitation energy E_x/A and mass A_0. The area of the squares is proportional to the intensity (from Ref. [37]).

given target, and given intervals of $Z_{\rm bound}$ may be reached with different targets but in collisions with different impact parameters. The partitioning, apparently, depends only on $Z_{\rm bound}$ and not on the impact parameter or target individually, as long as they populate a given range of $Z_{\rm bound}$.

The invariance of the fragmentation patterns, when plotted as a function of $Z_{\rm bound}$, suggests that the memory of the entrance channel and of the dynamics governing the primary interaction of the colliding nuclei is lost. This extends to other observables; the transverse-momentum widths of the fragments, as shown in Fig. 15.6, do not change with the bombarding energy, indicating that collective contributions to the transverse motion are small. The equilibration of the three kinetic degrees of freedom in the moving frame of the projectile spectator was confirmed by the analysis of the measured velocity spectra [36]. The square-root dependence on the atomic number Z implies kinetic energies nearly independent of Z and hence of the mass.

The success of the statistical multifragmentation models in describing the observed population of the partition space may be seen as a further argument for equilibration. Here the main task consists of finding an appropriate ensemble of excited nuclei to be subjected to the multi-fragment decay according to the model prescription. Starting from the entrance channel with models describing the primary phase of the collision may not necessarily provide sufficiently realistic ensembles, even though a good description of the fragment correlations was obtained with the quantum-molecular-dynamics model coupled to the statistical multifragmentation model [40]. An alternative method consists of using empirical ensembles derived by searching for an optimum reproduction of the observed partitioning. Near perfect descriptions of the measured correlations, including their dispersions around the mean behaviour, can be achieved [37, 41]. The mathematical procedure of backtracing allows for studying the uniqueness of the obtained solutions and their sensitivities to the observables that were used to generate them [42]. As an example, the ensemble derived empirically for the reaction ^{197}Au + ^{197}Au at 1000 MeV per nucleon is shown in Fig. 15.7. It extends over wide ranges of mass and excitation energy with both quantities being correlated as expected within the participant-spectator picture.

The spectator source, well localized in rapidity [36] and, apparently, exhibiting so many signs of equilibration, seems an excellent candidate for studying the nuclear phase diagram. Limitations arise from the fact that nucleons and very light particles from the early reaction stages may appear at spectator rapidities. Their contributions are difficult to suppress or to identify which makes it difficult to extract global variables such as the excitation energy of the system at the equilibrium stage. We will address this point in more detail when discussing the caloric curve of nuclei.

15.5 Measurement of Temperature

When measuring the temperature of excited nuclear systems one has to keep in mind that nuclei are closed systems with no external heat bath. Consequently, the temperature of the system cannot be pre-determined but has to be reconstructed from its decay products. For a microcanonical ensemble, the thermodynamic temperature of a system may be uniquely defined in terms of the total-energy state density. An experimental determination of the state density and of its energy dependence is, however, hitherto impossible, except at very low excitations where this method is actually being used [43]. Nuclear temperature determinations, therefore, take recourse to 'simple' observables of specific degrees of freedom which constitute a good approximation to the true thermodynamic temperature. In the canonical limit, the system may be seen as the heat bath for the chosen probe whose response is measured.

Several techniques have been developed for the determination of temperatures of excited nuclear systems [44]. In the work leading to the caloric curve of nuclei the method suggested by Albergo *et al.* [13] following earlier considerations of Hoyle [45] has been used. It is based on the assumption of chemical equilibrium and requires the measurement of double ratios of isotopic yields.

In the limit of thermal and chemical equilibrium, the double ratio R built from the yields Y_{i} of two pairs of nuclides with the same differences in neutron and proton numbers is given by

$$R = \frac{Y_1/Y_2}{Y_3/Y_4} = a \cdot \exp(((B_1 - B_2) - (B_3 - B_4))/T) = a \cdot \exp(\Delta B/T) \quad (15.4)$$

where B_{i} denotes the binding energy of particle species i and the constant a contains the mass numbers and internal partition sums. The chemical potential appearing in the expression for single isotope ratios (Eq. 15.2) cancels in the appropriately chosen double ratio. The expression can therefore be solved with respect to the temperature T provided the internal partition sums are known. The approximation usually made to circumvent this difficulty is to use the corresponding expression for the population of the ground states of the four isotopes, i.e. with the spin degeneracy factors for the ground states, and to treat modifications due to decays of higher-lying states as a perturbation. The problem of sequential decay, presently one of the main limitations of temperature measurements, will be discussed in more detail below.

A meaningful temperature scale can only be derived if the ratio R is sufficiently sensitive to the temperature of the system. By differentiating Eq. 15.4 we see that a relative error of the double yield ratio $\Delta R/R$ results in a relative modification of the extracted temperature by

$$\frac{\Delta T}{T} = -\frac{T}{\Delta B} \cdot \frac{\Delta R}{R}. \quad (15.5)$$

Thus, a stability of this thermometer against uncertainties of $\Delta R/R$ will only result if the binding energy difference $\Delta B = (B_1 - B_2) - (B_3 - B_4)$ is larger than the typical temperature to be measured. The analysis by Tsang *et al.* [46] of more than 1000 possible isotope thermometers for the same reaction supports this rule of thumb.

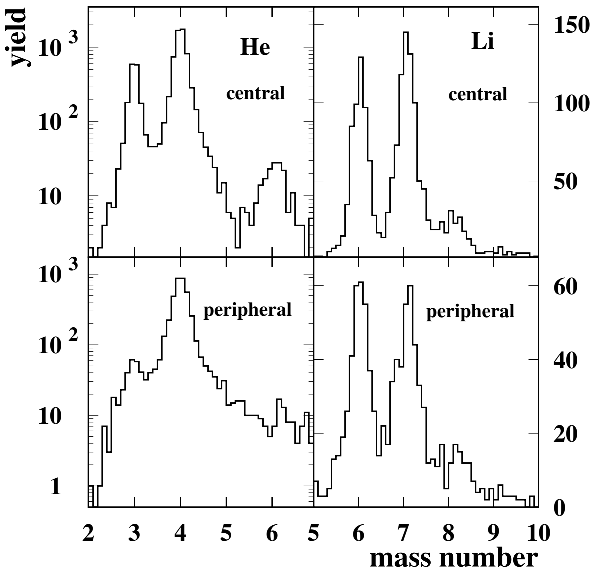

Figure 15.8: Mass spectra of He fragments (left panel) and Li fragments (right panel) from the projectile spectator following ^{197}Au + ^{197}Au collisions at E/A = 600 MeV. The upper and lower panels correspond to central and peripheral collisions, respectively (from Ref. [47]).

Particularly large values for ΔB are obtained if a $^3He/^4He$ ratio is involved because the difference in binding energy of the two helium isotopes is 20.6 MeV. It may be combined with, e.g., the lithium yield ratio ^{6}Li/^{7}Li or with the hydrogen yield ratios p/d or d/t. Mass spectra for helium and lithium isotopes, measured for the reaction ^{197}Au + ^{197}Au at E/A = 600 MeV with the ALADIN spectrometer, are shown in Fig. 15.8. The strong variation of the ^{3}He yields reflects the sensitivity of this less strongly bound nuclide to the variation of the temperature with impact parameter.

Solving Eq. 15.4 for this case of $^3He/^4He$ and ^{6}Li/^{7}Li and in the ground-state approximation yields the following expression:

$$T_{\rm HeLi,0} = 13.3 MeV/\ln(2.2\frac{Y_{^6{\rm Li}}/Y_{^7{\rm Li}}}{Y_{^3{\rm He}}/Y_{^4{\rm He}}}). \qquad (15.6)$$

The subscript 0 of $T_{\rm HeLi,0}$ is meant to indicate that Eq. 15.6 is strictly valid only for the ground-state population of the considered isotopes at the

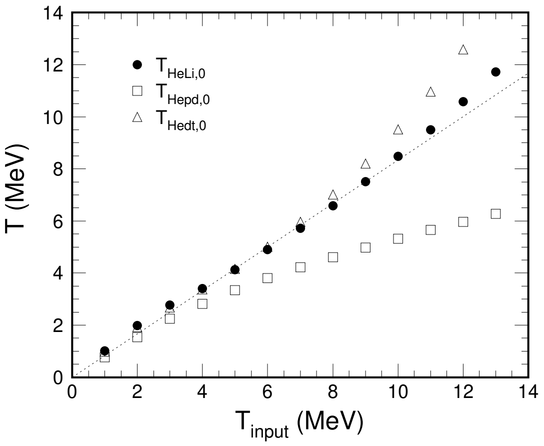

Figure 15.9: Temperatures $T_{\mathrm{HeLi},0}$, $T_{\mathrm{Hepd},0}$, and $T_{\mathrm{Hedt},0}$, according to the quantum statistical model, as a function of the input temperature T_{input}. A breakup density $\rho/\rho_0 = 0.3$ is assumed. The dotted line represents the linear relation $T_{\mathrm{input}}/1.2$ (from Ref. [37]).

breakup stage. The experimentally measured yields, however, contain all contributions from γ-unstable higher-lying states of the same isotope and from particle decays of other isotopes feeding the ground or γ-unstable states. In the work of the ALADIN collaboration [48], the expected magnitude of this effect was investigated by performing calculations with the quantum-statistical model [22, 23], a sequential-evaporation model [49], and a statistical multifragmentation model [50]. The primary fragmentation process is treated very differently in these models but they all follow explicitly the sequential decays of excited primary products.

As an example, results obtained with the quantum statistical model are shown in Fig. 15.9. The assumed breakup density is $\rho/\rho_0 = 0.3$ with ρ_0 denoting the saturation density. Despite the strong feeding of the light particle yields through secondary decays, the relation between the input temperature of the model and $T_{\mathrm{HeLi},0}$ as well as $T_{\mathrm{Hedt},0}$ was found to be almost linear. Other temperature probes, as illustrated for $T_{\mathrm{Hepd},0}$ in the figure, may be more strongly affected by sequential decays. Variations of the input density within reasonable limits in this model and the comparison with results obtained with the other decay models suggested that the accuracy of these estimates may lie within $\pm$ 15%. In order to account for the systematic

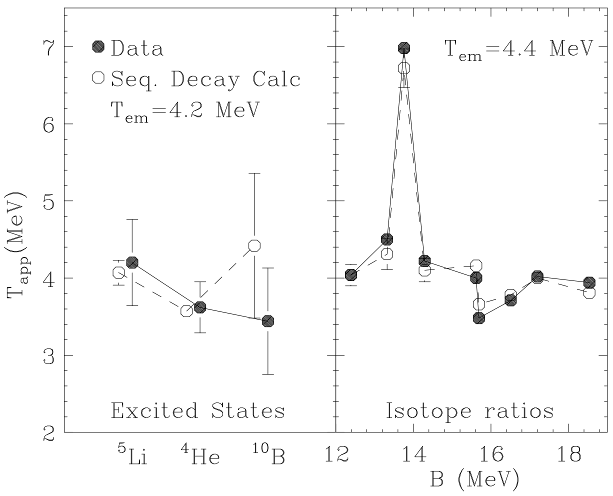

Figure 15.10: Apparent temperatures obtained from relative populations of excited states for ^{5}Li, ^{4}He, and ^{10}B nuclei (left panel) and from isotopic ratios (right panel, $T_{\mathrm{HeLi},0}$ is given by the data point at B = 13.3 MeV). The closed points are the data and the open points are the predictions of sequential decay calculations (from Ref. [57]).

deviation from unity, a constant calibration factor $T_{\mathrm{HeLi}} = 1.2 \cdot T_{\mathrm{HeLi},0}$ was adopted (corresponding to the dotted line in Fig. 15.9).

The consequences of sidefeeding from higher lying states have also been investigated by other groups with different methods (see, e.g., Refs. [24, 25, 51, 52] and references given therein). The results differ considerably in magnitude as well as in the sign of the required correction [24, 53] and, in some cases, exceed the ±15% margin quoted above [25]. The treatment of the continuum part of the excitation spectrum of emitted fragments is conceptually and practically difficult [25, 51] and, furthermore, each isotope thermometer will require an individual calibration (Fig. 15.9 and Refs. [54, 55]). It is obvious that quantitative experimental information on the amount of sequential feeding will be needed, such as recently obtained for ^{129}Xe + Sn reactions [56], and that experimental cross comparisons with alternative thermometers are mandatory in order to possibly reduce the uncertainties of the isotopic temperature scale.

A first cross comparison of the T_{HeLi} thermometer with excited-state temperatures deduced from excited state populations of lithium, beryllium and boron isotopes for the ^{36}Ar + ^{197}Au reaction at 35 MeV per nucleon gave compatible results [55]. A similar consistency was also observed for central collisions of the heavier Au + Au system at the same energy [57]. The quality of the agreement between the different thermometers investigated in the latter reaction is shown in Fig. 15.10. In the nomenclature used there, a distinction is made between the 'true' emission temperature at breakup $T_{\rm em}$ and the uncorrected apparent temperature $T_{\rm app}$ obtained with a particular thermometer, such as $T_{\rm HeLi,0}$ in Eq. 15.6 [58]. All temperature values, deduced either from relative populations of states (left panel) or from isotopic yield ratios (right panel), are consistent with an emission temperature of 4.3 ± 0.1 MeV. The figure also demonstrates that the sequential-decay calculations used for this case reproduce the observed behaviour of the apparent temperatures rather well, including the large excursion of the apparent isotope temperature deduced from ^{3,4}He and ^{9,10}Be ($\Delta B = 13.8$ MeV). This anomaly has been traced down to the imbalance in the number of low-lying excited states in the ^{9,10}Be pair [59]; it reflects the potentially dramatic influence of sequential decays in special cases.

A cross calibration over a wider range of excitation energies and reaction types was performed by studying central ^{197}Au + ^{197}A collision at 50 to 200 MeV per nucleon incident energy with the ALADIN spectrometer. For this purpose, the setup had been supplemented by three hodoscopes and several high-resolution telescopes positioned at angles close to mid-rapidity [60]. The angular resolution and granularity of the hodoscopes was optimized in order to permit the identification of excited particle unstable resonances in light fragments from the correlated detection of their decay products. Yields of isotopically resolved light fragments were measured with the individual telescopes which each consisted of three Si detectors of increasing thickness backed by a CsI(Tl) scintillation detector.

The obtained values for two isotope and three excited-state temperatures are given in Fig. 15.11. The isotope temperatures $T_{\rm HeLi}$ and $T_{\rm Hedt}$ were derived as described above, and a correction factor of 1.2 was applied in order to account for the effects of sequential feeding. Excited-state temperatures were determined for ^{4}He, ^{5}Li, and ^{8}Be, fragments with two widely separated states for which modifications of the apparent emission temperatures due to feeding were expected to be small (Fig. 15.10 and Refs. [61, 62]).

At 50 MeV per nucleon, all temperature values coincide within the interval T = 4 to 6 MeV in good agreement with the result of Huang *et al.*

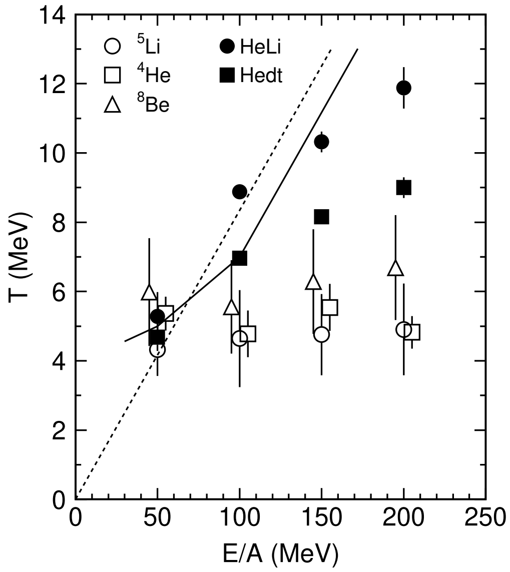

Figure 15.11: Measured isotope temperatures (full symbols) and excited-state temperatures (open symbols) as a function of the incident energy per nucleon. The indicated uncertainties are mainly of systematic origin. The meaning of the lines is explained in the text (data from [60]).

[57] obtained at 35 MeV per nucleon (Fig. 15.10). With rising beam energy, however, the isotope temperatures rise linearly up to $T_{\rm HeLi} \approx 12$ MeV and $T_{\rm Hedt} \approx 9$ MeV at 200 MeV per nucleon (closed symbols). The excited-state temperatures, on the other hand, appear to be virtually independent of the bombarding energy. They scatter closely around their individual mean values of about 4.5 MeV up to 6 MeV for the three cases. The same striking divergence of the two types of thermometers has been made for central ^{86}Kr + ^{93}Nb reactions [63] and for spectator reactions in ^{197}Au + ^{197}Au at 1000 MeV per nucleon [64].

Lacking at the moment a quantitative explanation of this surprising observation, it might be instructive to recall a similar phenomenon during the cosmic big-bang. Also there different degrees of freedom freeze out at various stages of the big-bang evolution, hence signaling different temperatures. Of course, this cooling is intimately related to the existence of collective radial flow. It may, therefore, not be too surprising that the discrepancy between the two thermometers, in this case, emerges at incident energies exceeding 50 MeV per nucleon at which radial collective flow starts to represent a significant part of the available collision energy [65]. Rather crude estimates for the expected breakup temperatures if flow is taken into account are given by the lines in Fig. 15.11. They qualitatively indicate the tendency exhibited by the isotope temperatures. The interpretation of the excited-state temperatures should also consider that the resonances used for the temperature evaluation are very specific quantum states with widths of 1 MeV or less. They are unlikely to exist in the nuclear medium in identical forms [66, 67, 68]. In the case of volume breakup, the asymptotic states that finally will be observed can develop and survive only at very low densities that may not be experienced by the cluster before it is effectively emitted into vacuum. Excited-state temperatures may thus represent the internal fragment temperatures at the very final stages of the fragmentation process. The obtained mean value near 5 MeV corresponds well to results of dynamical calculations based on transport models [70].

Apparent temperatures deduced from purely thermal interpretations of the Maxwellian-like kinetic-energy spectra are in clear disagreement with the isotope temperatures. There are many effects that may influence the kinetic energies in these reactions, such as sequential decay, collective motion, Coulomb interaction, preequilibrium emissions and Fermi motion. For spectator decays following ^{197}Au + ^{197}Au collisions, e.g., the kinetic temperatures are of the order of 15 to 20 MeV and much larger than the breakup temperatures discussed so far. It has recently been shown, however, that taking into account the effect of the nucleonic Fermi motion within the colliding nuclei will reconcile these seemingly contradictory observations [71, 72].

15.6 A Caloric Curve of Nuclei

Caloric curve is the term commonly adopted for a relation between temperature T and energy E. In thermodynamics, the caloric equation of state is given by the function $E(T)$ under well defined conditions as, e.g., fixed volume and particle number in the simplest case. Here we will speak of a caloric curve of nuclei in the looser sense in that we use our experimental means to change the energy content of a nuclear system and simultaneously measure its temperature [73]. The obvious motivation for this endeavour is

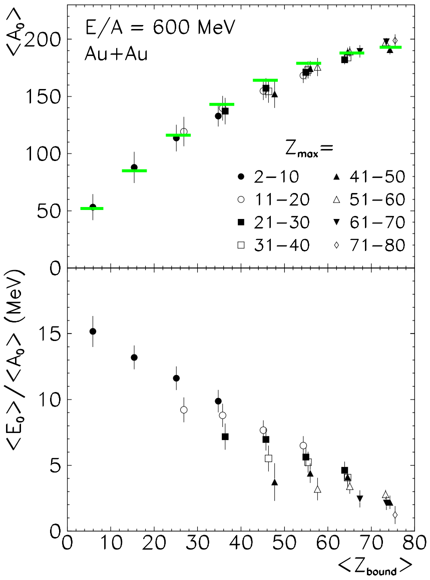

Figure 15.12: Reconstructed average mass $\langle A_0 \rangle$ (top) and excitation energy $\langle E_0 \rangle / \langle A_0 \rangle$ (bottom) of the decaying spectator system as functions of $Z_{\rm bound}$ and $Z_{\rm max}$. The data symbols represent averages over 10-unit-wide bins in these two quantities as indicated. The shaded horizontal bars (top panel) represent the masses according to the participant-spectator model at the empirical impact parameter deduced from $d\sigma/dZ_{\rm bound}$ (from Ref. [48]).

provided by the hope of establishing a link to the hypothetical liquid-gas phase transition in extended nuclear matter [74].

At relativistic energies, only small fractions of the initial collision energy are converted into excitation energy of the spectator. The energy deposition there can only be reconstructed from the exit-channel configuration which, however, requires a complete knowledge of all decay products with their atomic numbers, masses, and kinetic energies and including neutrons. Since this is not easy to obtain, at the least event by event, assumptions and approximations have to be made.

A method to determine the excitation energy from the experimental data along this line was first presented by Campi *et al.* [75] and applied to the ^{197}Au + Cu data measured by the ALADIN collaboration in their first experiment [39]. The caloric curve presented in Ref. [48] was constructed from the more recent data for the ^{197}Au + ^{197}Au reaction at 600 MeV per nucleon. Here also experimental information on neutron production, collected with LAND, was used. Hydrogen isotopes were not detected and assumptions concerning the overall N/Z ratio of the spectator, the intensity ratios of protons, deuterons, and tritons, and the kinetic energies of hydrogen isotopes had to be made. The masses of the heavier fragments were not measured with sufficient precision and assumed to follow the EPAX parameterization [76]. The uncertainties resulting from the variation of these quantities within reasonable limits were included in the errors assigned to the results.

The spectator masses A_0 and the specific excitation energies E_0/A_0, obtained from this analysis, are given in Fig. 15.12 as functions of $Z_{\rm bound}$ and $Z_{\rm max}$, with $Z_{\rm max}$ denoting the maximum atomic number detected within an event. The mean mass $\langle A_0 \rangle$ decreases with decreasing $Z_{\rm bound}$, in good agreement with the expectations from the geometric participant-spectator model [35]. Within a given bin of $Z_{\rm bound}$, $\langle A_0 \rangle$ is fairly independent of $Z_{\rm max}$. The smallest mean spectator mass in the bin of $Z_{\rm bound} \leq 10$ is $\langle A_0 \rangle \approx 50$. The excitation energy E_0 appears to be a function of both $Z_{\rm bound}$ and $Z_{\rm max}$; events with smaller $Z_{\rm max}$, i.e. the more complete disintegrations, correspond to the higher excitation energies. The maximum number of fragments, observed at $Z_{\rm bound} \approx 40$, is associated with initial excitation energies of $\langle E_0 \rangle / \langle A_0 \rangle \approx 8$ MeV. With decreasing $Z_{\rm bound}$ the deduced excitation energies reach up to $\langle E_0 \rangle / \langle A_0 \rangle \approx 16$ MeV.

The pairwise correlation of the isotope temperature, deduced as described in the last section, with the excitation energy leads to the caloric curve shown in Fig. 15.13. Besides the data from projectile decays following ^{197}Au + ^{197}Au collisions at 600 MeV per nucleon, results from earlier experiments with ^{197}Au targets at intermediate energies 30 to 84 MeV per nucleon (c.f. Section 15.2) and for compound nuclei produced in the ^{22}Ne + ^{181}Ta reaction are included. For the light-ion induced reactions at intermediate energies, the excitation energy of the target residues was obtained by subtracting the energy lost in preequilibrium emissions from the collision energy while, in the compound case, it was assumed to be equal to the collision energy.

We first like to draw attention to the fact that the whole range of reaction channels from compound evaporation to near vaporization can be covered with a single temperature observable. The required helium and lithium isotopes are still produced in sufficient quantity at these extreme ends of the range of excitation energies. We further notice the consistency of the

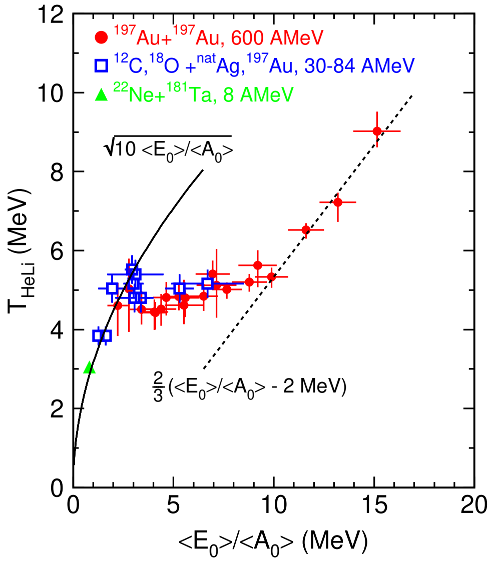

Figure 15.13: Caloric curve of nuclei as constituted by the temperature $\mathrm{T_{HeLi}}$ as a function of the excitation energy per nucleon. The lines are explained in the text (from Ref. [48]).

data obtained for different types of reactions, suggesting that the smooth S-shaped curve may represent a more general property of excited nuclei. In fact, at low energies, the deduced temperatures T_{HeLi} follow the sqare-root behaviour of a Fermi-liquid, as represented by the full line calculated for a level density parameter $a = A/10$ MeV^{-1}. At high excitation energies, the rise of the temperature seems to approach a linear function with the slope 2/3 of a classical gas. In the limit of a free nucleon gas, the offset should be $\approx$ 8 MeV, corresponding to the mean binding energy of nuclei. A smaller offset may be caused by the finite density at freeze-out and by the finite fraction of bound clusters and fragments of intermediate mass that are present even at these high excitation energies. The offset of 2 MeV is consistent with a breakup density ρ/ρ_0 between 0.15 and 0.3 [48].

Within the range of $\langle E_0\rangle/\langle A_0\rangle$ from 3 MeV to 10 MeV, the temperature increases very little while the system passes from the 'liquid' regime, governed by the degrees of freedom of a heavy residue, to that of the 'vapor' of light fragments and particles. This transition in the dominant characteris-

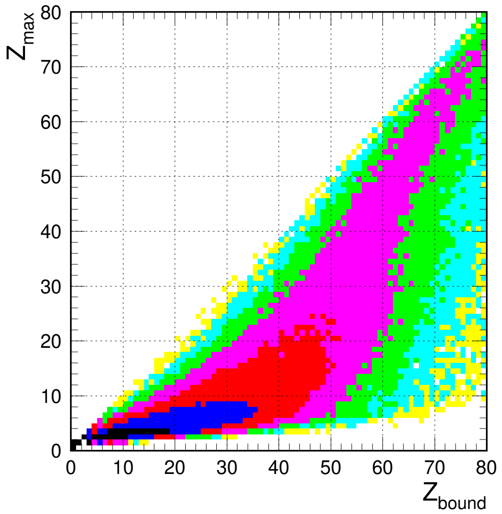

Figure 15.14: Z_{max}-versus-Z_{bound} distribution measured in the reaction ^{197}Au + ^{197}Au at 1000 MeV per nucleon. Conventional fission events are removed, the shadings follow a logarithmic scale (from Ref. [77]).

tics of the reaction channel is illustrated in Fig. 15.14 which shows the event distribution in the Z_{max}-versus-Z_{bound} plane. At large Z_{bound}, corresponding to small excitation energies, the ridge line starts at $Z_{\mathrm{max}} \approx Z_{\mathrm{bound}}$, i.e. with events containing only one large fragment or heavy residue. The most probable Z_{max} then drops fairly rapidly near $Z_{\mathrm{bound}} \approx 50$ and approaches very small values at the smallest Z_{bound}. The observation of $Z_{\mathrm{max}} \ll Z_{\mathrm{bound}}$ in this region of large excitation energies implies that the system has disintegrated into a larger number of smaller fragments. The energy needed for the formation of smaller constituents, correspondingly, limits the rise of the temperature.

The qualitative interpretation of the caloric curve along these lines is motivated by its reminiscence of what we expect for a first-order phase transition. It has to be refined and possibly confirmed with model studies. Statistical multifragmentation models have been used to identify the individual contributions to the total excitation energy and to quantify the origin of the second rise at $E_x/A \approx 10$ MeV [27, 78]. It was found that the internal degrees of freedom of fragments of intermediate mass are still quite important at these high excitations [27]. Transport theoretical approaches, based on antisymmetrized molecular-dynamics models, give the possibility to study nuclear systems at finite pressure [79, 80]. Caloric curves obtained in this way in model experiments include a rise at high excitations that has been shown to correspond to a nucleon gas with Van-der-Waals properties [80].

Alternative interpretations, in particular for the temperature rise at the highest energies, have been presented by several groups. In the interpretation of Natowitz *et al.* [81], the variation of the system mass (Fig. 15.12) is seen as the primary reason for the observed variation of the temperature and related to the mass dependence of the temperatures limiting the stability of excited nuclei [82]. In the expansion scenario modeled by Papp and Nörenberg [33], the temperatures in the plateau region are found to be consistent with a spinodal decomposition in the dynamically unstable region of the temperature-versus-density plane. The upbend at high excitation energies, in this model, indicates a concentration of the deduced breakup densities at a minimum value around $\rho/\rho_0 \approx 0.3$.

Another line of interpretation emphasizes the time dependence of the emission process. The time evolution has been studied with the expanding-emitting source model which assumes statistical emissions from an expanding and thereby cooling source [83]. According to these calculations, the less bound nuclei are more likely to be emitted at earlier reaction times, with the effect that integrated yield ratios represent a complex convolution of the temperature profile and the emission probabilities as a function of the reaction time [52]. Temperatures obtained from integrated yield ratios, consequently, have the character of weighted mean values over finite distributions. Differential analyses have been performed in order to extract cooling curves [84] or to obtain temperature values for fixed reaction times [85]. For some reactions a systematic difference of the kinetic energy spectra of the ^{3,4}He nuclei has been observed, suggesting that the two isotopes originate from different reaction stages [86, 87]. It is therefore desirable to extend the range of temperature observables to other combinations of isotopes that do not include the helium nuclei. The T_{BeLi} temperature, derived from the ^{7,9}Be and ^{6,8}Li isotope ratios appears to be a promising candidate; the second rise at high excitation energies is also seen with this observable [88].

The discussion clearly shows that asking for a final interpretation of the caloric curve of nuclei would be premature at the present time. Furthermore, ongoing analyses and new data have also led to small modifications of the originally published curve. As a result of previously not included experi-

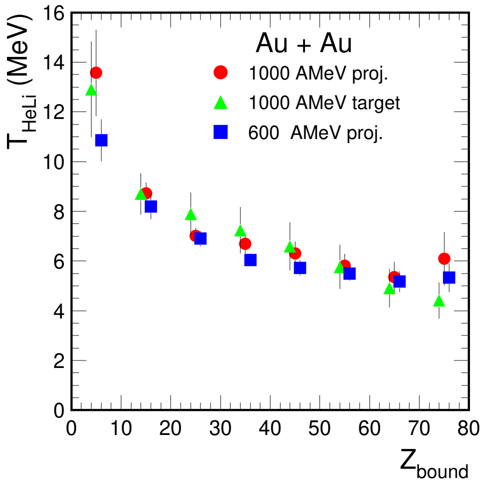

Figure 15.15: Temperatures $T_{\rm HeLi}$ for target (E/A = 1000 MeV) and projectile spectators (E/A = 600 and 1000 MeV) as a function of $Z_{\rm bound}$. The data symbols represent averages integrated over $Z_{\rm max}$ and over 10-unit wide bins of $Z_{\rm bound}$ (from Ref. [77]).

mental information and corrections, the temperatures deduced for projectile fragments in the ^{197}Au + ^{197}Au reaction at 600 MeV per nucleon have increased by between 10% and 20% [37]. The new temperature values $T_{\rm HeLi}$ are shown in Fig. 15.15 as a function of $Z_{\rm bound}$ and, unlike Fig. 15.13, averaged over $Z_{\rm max}$. They are compared to the results obtained at 1000 MeV per nucleon, for both the projectile and target spectators. For the target spectator, isotopic yields were measured at $\theta_{\rm lab}$ = 150° with a four-element telescope while $Z_{\rm bound}$ was determined for the coincident projectile decay with the ALADIN time-of-flight wall. The agreement with the temperatures obtained for the projectile decay at the same energy is expected from the symmetry of the collision and only illustrates the accuracy achieved in these experiments. The coinciding results for 600 and 1000 MeV per nucleon incident energy, on the other hand, indicate an invariance with respect to the bombarding energy that is well known from other observables (Section 15.4). Calculations with the statistical multifragmentation model, using the ensemble of excited spectator nuclei shown in Fig. 15.7, are in good agreement with these measurements [37]. The simultaneous reproduction of the observed charge partitions and of this temperature-sensitive observable represents a necessary requirement for a consistent statistical description of the spectator fragmentation.

More recent data and analyses have also shown that the excitation energies obtained from calorimetry do not exhibit a similar invariance with respect to the incident energy. It was found that the mean kinetic energies of neutrons, measured at three bombarding energies with LAND, increase considerably with the bombarding energy [89]. Together with the contribution of the protons, this leads to a difference of about 40% in the reconstructed excitation energy for the collisions at 600 and 1000 MeV per nucleon. Most likely, the experimental nucleon yields contain contributions from earlier reaction stages even if they are measured in the kinematic regimes corresponding to spectator decays. This may also provide the explanation for the excess of the experimentally determined energies over those obtained from backtracing with the statistical multifragmentation model (Figs. 15.7, 15.12, and Ref. [36]). Detailed studies of light particle emissions in these reactions, including excitation functions, will be needed in order to disentangle the various sources of light particles. At present, this uncertainty prevents the construction of a fully invariant caloric curve from spectator decays.

With the same or similar techniques caloric curves have been derived by other groups for other types of reactions [85, 90, 91, 92, 93]. The transition from the liquid branch to a plateau-like behaviour, coinciding with the onset of fragment production, seems to be a general feature of all of these curves. The second rise, however, is not seen as pronounced as for the ^{197}Au + ^{197}Au spectator reactions (Figs. 15.13,15.15). With lighter projectiles, the cross sections for reaching the high excitation energies at which this rise occurs are rather small (cf. Fig. 15.5). On the other hand, the vaporization of light systems into hydrogen and helium isotopes, as observed for the ^{36}Ar + ^{58}Ni reaction at 95 MeV per nucleon [94], has been described with a chemical-equilibrium model and temperatures of up to 24 MeV [25].

15.7 Concluding Remarks

This chapter has been meant to illustrate the usefulness of isotopic yield ratios for a statistical description of heavy-ion reactions. The main topics were the questions of how to obtain evidence for equilibration and of how to actually measure thermodynamical variables. From there a very natural path has led to phase transitions in finite nuclei, a topic of highest current interest. It is obvious that none of these subjects has been covered exhaustively, and we refer the reader to the cited literature and to the relevant articles collected in this volume.

The underlying concept of equilibrated breakup states necessarily constitutes an idealization in view of the rapid dynamic evolution of energetic reaction processes. Its limitations were evident in the discussion of multifragment emissions, most notably in the comparison of the different temperature observables. The dominant role of phase space, on the other hand, is apparent from the successful description of a variety of global characteristics of these reactions that is possible with the assumption of a statistical breakup.

The increasing availability of secondary beams for nuclear reactions will allow future studies of isospin degrees of freedom to be extended over a wider range of neutron-to-proton asymmetries. The two-fluid nature of nuclear matter promises new phenomena to be seen in experiments with asymmetric nuclei, as discussed elsewhere in this volume. Isotopic yield ratios can be expected to remain in the center of interest as important observables probing the source composition as well as its thermodynamical properties. It is also not excluded that spectator reactions at high energies will prove unique for producing globally equilibrated asymmetric systems over the desired wide range of excitation energies.

The authors would like to thank their colleagues of the ALADIN collaboration and at the GSI for support and discussions during the preparation of this manuscript.

Bibliography

[1] R. Wada *et al.*, Phys. Rev. Lett. 58, 1829 (1987)

[2] F. Deák *et al.*, Phys. Rev. C 43, 2432 (1991)

[3] L.N. Andronenko *et al.*, Z. Phys. A 350, 1 (1994)

[4] J. Mougey *et al.*, Phys. Lett. 105B, 25 (1981)

[5] D. Guerreau *et al.*, Phys. Lett. 131B, 293 (1983)

[6] R. Lucas *et al.*, Nucl. Phys. A 464, 172 (1987)

[7] For a review see, e.g., B. Borderie *et al.*, Ann. Phys. Fr. 15, 287 (1990)

[8] S.J. Yennello *et al.*, Phys. Lett. B 321, 15 (1994)

[9] H. Johnston *et al.*, Phys. Lett. B 371, 186 (1996)

[10] H. Johnston *et al.*, Phys. Rev. C 56, 1972 (1997)

[11] F. Rami *et al.*, Phys. Rev. Lett. 84, 1120 (2000)

[12] A.Z. Mekjian, Phys. Rev. C 17, 1051 (1978)

[13] S. Albergo *et al.*, Il Nuovo Cimento 89 A 1 (1985)

[14] H.W. Barz *et al.*, Phys. Lett. B 211, 10 (1988)

[15] W. Trautmann *et al.*, Nucl. Phys. A 471, 191c (1987)

[16] V.I. Bogatin *et al.*, Yad. Fiz. 19, 32 (1974) [Sov. J. Nucl. Phys. 19, 16 (1974)]

[17] O.V. Lozhkin and W. Trautmann, Phys. Rev. C 46, 1996 (1992)

[18] V. Avdeichikov *et al.*, Physica Scripta 50, 624 (1994)

[19] G.J. Kunde *et al.*, Phys. Rev. Lett. 77, 2897 (1996)

[20] H.S. Xu *et al.*, preprint MSUCL-1137 (1999)

[21] V.I. Bogatin *et al.*, Yad. Fiz. 31, 845 (1980) [Sov. J. Nucl. Phys. 31, 436 (1980)]; 34, 104 (1981) [34, 59 (1981)]

[22] D. Hahn and H. Stöcker, Nucl. Phys. A 476, 718 (1988)

[23] J. Konopka *et al.*, Phys. Rev. C 50, 2085 (1994)

[24] Z. Majka *et al.*, Phys. Rev. C 55, 2991 (1997)

[25] F. Gulminelli and D. Durand, Nucl. Phys. A 615, 117 (1997)

[26] D.H.E. Gross, Rep. Prog. Phys. 53, 605 (1990)

[27] J.P. Bondorf *et al.*, Phys. Rep. 257, 133 (1995)

[28] S. Fritz *et al.*, Phys. Lett. B 461, 315 (1999)

[29] W.-C. Hsi *et al.*, Phys. Rev. Lett. 79, 817 (1997)

[30] R. Trockel *et al.*, Phys. Rev. C 38, 576 (1988)

[31] C. Kuhn *et al.*, Phys. Rev. C 48, 1232 (1993)

[32] G.F. Bertsch, Nucl. Phys. A 400, 221c (1983)

[33] G. Papp and W. Nörenberg, APH Heavy Ion Physics 1 (1995) 241

[34] For a introductory survey see, e.g., W. Trautmann, *in*: "Correlations and Clustering Phenomena in Subatomic Physics," edited by M.N. Harakeh *et al.*, Plenum Press, New York (1997)

[35] J. Gosset *et al.*, Phys. Rev. C 16, 629 (1977)

[36] A. Schüttauf *et al.*, Nucl. Phys. A 607, 457 (1996)

[37] Hongfei Xi *et al.*, Z. Phys. A 359, 397 (1997)

[38] C.A. Ogilvie *et al.*, Phys. Rev. Lett. 67, 1214 (1991)

[39] P. Kreutz *et al.*, Nucl. Phys. A 556, 672 (1993)

[40] J. Konopka *et al.*, Prog. Part. Nucl. Phys. 30, 301 (1993)

[41] A.S. Botvina *et al.*, Nucl. Phys. A 584, 737 (1995)

[42] P. Désesquelles *et al.*, Nucl. Phys. A 604, 183 (1996)

[43] E. Melby *et al.*, Phys. Rev. Lett. 83, 3150 (1999)

[44] D.J. Morrissey *et al.*, Ann. Rev. Nucl. Part. Science 44, 65 (1994)

[45] F. Hoyle, The synthesis of the elements from hydrogen, Monthly Notices of the Royal Astronom. Soc. 106, 343 (1946)

[46] M.B. Tsang *et al.*, Phys. Rev. Lett. 78, 3836 (1997)

[47] T. Möhlenkamp *et al.*, *Proceedings of the XXXIII International Winter Meeting on Nuclear Physics*, Bormio, 1995, edited by I. Iori (Ricerca Scientifica ed Educazione Permanente, Milano, 1995), p. 383

[48] J. Pochodzalla *et al.*, Phys. Rev. Lett. 75, 1040 (1995)

[49] R.J. Charity *et al.*, Nucl. Phys. A 483, 371 (1988)

[50] D.H.E. Gross *et al.*, Phys. Rev. Lett. 56, 1544 (1986)

[51] Hongfei Xi *et al.*, Phys. Rev. C 54, R2163 (1996)

[52] V.E. Viola *et al.*, Phys. Rev. C 59, 2660 (1999)

[53] H.F. Xi *et al.*, Phys. Lett. B 431, 8 (1998)

[54] A. Kolomiets *et al.*, Phys. Rev. C 54, R472 (1996)

[55] M.B. Tsang *et al.*, Phys. Rev. C 53, R1057 (1996)

[56] N. Marie *et al.*, Phys. Rev. C 58, 256 (1998)

[57] M.J. Huang *et al.*, Phys. Rev. Lett. 78, 1648 (1997)

[58] The term emission temperature is sometimes exclusively used for temperatures extracted from relative populations of excited states, see e.g. Ref. [73]

[59] J. Bondorf *et al.*, Phys. Rev. C 58, R27 (1998)

[60] V. Serfling *et al.*, Phys. Rev. Lett. 80, 3928 (1998)

[61] J. Pochodzalla *et al.*, Phys. Rev. C 35, 1695 (1987)

[62] C. Schwarz *et al.*, Phys. Rev. C 48, 676 (1993)

[63] H.F. Xi *et al.*, Phys. Rev. C 58, R2636 (1998)

[64] C. Groß, PhD thesis, Universität Frankfurt, 1998

[65] W. Reisdorf and H.G. Ritter, Annu. Rev. Nucl. Part. Science 47, 663 (1997)

[66] M. Schmidt *et al.*, Ann. Phys. (N.Y.) 202, 57 (1990)

[67] T. Alm *et al.*, Phys. Rev. C 53, 2181 (1992)

[68] P. Danielewicz and Q. Pan, Phys. Rev. C 46, 2002 (1992)

[69] P.B. Gossiaux *et al.*, Nucl. Phys. **A619**, 379 (1997)

[70] C. Fuchs *et al.*, Nucl. Phys. A 626, 987 (1997)

[71] T. Gaitanos *et al.*, Phys. Lett. B 478, 79 (2000)

[72] T. Odeh *et al.*, Phys. Rev. Lett. 84, 4557 (2000)

[73] For a more comprehensive status report, see J. Pochodzalla, Prog. Part. Nucl. Phys. 39, 443 (1997)

[74] For a recent review of the field see, e.g., Proceedings of the International Workshop XXVII on Gross Properties of Nuclei and Nuclear Excitations, Hirschegg, Austria, edited by H. Feldmeier *et al.* (GSI, Darmstadt, 1999)

[75] X. Campi *et al.*, Phys. Rev. C 50, R2680 (1994)

[76] K. Sümmerer *et al.*, Phys. Rev. C 42, 2546 (1990)

[77] T. Odeh, PhD thesis, Universität Frankfurt, 1999

[78] Al.H. Raduta and Ad.R. Raduta, Nucl. Phys. A 647, 12 (1999)

[79] J. Schnack and H. Feldmeier, Phys. Lett. B 409, 6 (1997)

[80] Y. Sugawa and H. Horiuchi, Phys. Rev. C 60, 064607 (1999)

[81] J.B. Natowitz *et al.*, Phys. Rev. C 52, R2322 (1995)

[82] P. Bonche *et al.*, Nucl. Phys. A 436, 265 (1986)

[83] W.A. Friedman *et al.*, Phys. Rev. C 42, 667 (1990)

[84] H.F. Xi *et al.*, Phys. Rev. C 57, 462 (1998)

[85] J. Cibor *et al.*, Phys. Lett. B 473, 29 (2000)

[86] R. Bougault *et al.*, in Ref. [74], p. 24

[87] W. Neubert and A.S. Botvina, Eur. Phys. J. A, in print (2000)

[88] W.F.J. Müller *et al.*, in Ref. [74], p. 200

[89] C. Groß, PhD thesis, Universität Frankfurt, 1999

[90] Y.-G. Ma *et al.*, Phys. Lett. B 390, 41 (1997)

[91] J.A. Hauger *et al.*, Phys. Rev. C 57, 764 (1998)

[92] K. Kwiatkowski *et al.*, Phys. Lett. B 423, 21 (1998)

[93] M. D'Agostino *et al.*, Nucl. Phys. A 650, 329 (1999)

[94] B. Borderie *et al.*, Eur. Phys. J. A 6, 197 (1999)